Quaternary Research 73 (2010) 541–549

Contents lists available at ScienceDirect

Quaternary Research

journal homepage: www.elsevier.com/locate/yqres

The East Asian monsoon during MIS 2 expressed in a speleothem $\delta^{18}O$ record from Jintanwan Cave, Hunan, China

Jason Cosford [a,*], Hairuo Qing [a], Yin Lin [b], Bruce Eglington [c], Dave Mattey [d], Yue Gau Chen [b], Meiliang Zhang [e], Hai Cheng [f]

[a] Department of Geology, University of Regina, Regina, SK, Canada S4S 0A2
[b] Department of Geosciences, National Taiwan University, Taipei, Taiwan (R.O.C.) 10611
[c] Saskatchewan Isotope Laboratory, Department of Geological Sciences, University of Saskatchewan, Saskatoon, SK, Canada S7N 5E2
[d] Department of Geology, Royal Holloway University of London, Egham, Surrey, TW20 0EX, UK
[e] Institute of Karst Geology, Chinese Academy of Geological Science, Guilin, China, 541004
[f] Department of Geology and Geophysics, University of Minnesota, Twin Cities, MN 55455, USA

ARTICLE INFO

Article history:
Received 16 April 2009
Available online 25 February 2010

Keywords:
Stalagmite
Oxygen isotopes
East Asian monsoon
Last glacial maximum

ABSTRACT

Stalagmite J1 from Jintanwan Cave, Hunan, China, provides a precisely dated, decadally resolved $\delta^{18}O$ proxy record of paleoclimatic changes associated with the East Asian monsoon from ~29.5 to 14.7 ka and from ~12.9 to 11.0 ka. At the time of the last glacial maximum (LGM), the East Asian summer monsoon weakened and then strengthened in response to changes in Northern Hemisphere insolation. As the ice sheets retreated the East Asian summer monsoon weakened, especially during Heinrich event H1, when atmospheric and oceanic teleconnections transferred the climatic changes around the North Atlantic to the monsoonal regions of Eastern Asia. A depositional hiatus between ~14.7 and 12.9 ka leaves the deglacial record incomplete, but an abrupt shift in $\delta^{18}O$ values at ~11.5 ka marks the end of the Younger Dryas and the transition into the Holocene. Comparisons of the J1 record to other Chinese speleothem records indicate synchronous climatic changes throughout monsoonal China. Further comparisons to a speleothem record from western Asia (Socotra Island) and to Greenland ice cores support hemispherical-scale paleoclimatic change. Spectral and wavelet analyses reveal centennial- and decadal-scale periodicities that correspond to solar frequencies and to oscillations in atmospheric and oceanic circulation.

Introduction

Climatic changes associated with the East Asian monsoon during marine isotope stage 2 (MIS 2) provide insight into the linkages between the East Asian monsoon and the global climate system. During this period of glacial conditions, which includes the last glacial maximum (LGM) and deglaciation, changes in insolation, atmospheric and oceanic circulation, and global ice volume influenced the strength and character of the East Asian monsoon, demonstrating that the East Asian monsoon is a key component of the global climate system (Wang et al., 2005). The timing and character of the response of the East Asian monsoon to these changes reflects the dominant climatic forcing mechanisms and global climatic teleconnections. Previous studies have demonstrated that the East Asian monsoon oscillated primarily in response to changes in Northern Hemisphere summer insolation (Wang et al., 2008) and to changes in ice volume (Ding et al., 1995), but over shorter millennial to centennial time scales, changes in atmospheric and oceanic conditions can override orbital and ice-volume forcing of monsoonal circulation (Zhou et al., 2008; Wu et al., 2009).

In this study, we present a decadally resolved speleothem (J1) $\delta^{18}O$ record spanning MIS 2 from Jintanwan Cave, Hunan, China. The J1 $\delta^{18}O$ record shows that the East Asian summer monsoon weakened and then strengthened during the LGM in response to insolation forcing and that, despite insolation forcing, the East Asian summer monsoon weakened during Heinrich event H1 in response to colder temperatures in northern high latitudes and changes in oceanic circulation. Higher frequency fluctuations on centennial and multi-decadal scales during the last glaciation are not as well understood. Unlike many other paleoclimatic archives that are hindered by low temporal resolution and age uncertainties, speleothem isotope records have the potential to resolve higher frequency fluctuations in East Asian monsoonal circulation during this period, but few such records have been reported. Several spectral and wavelet analyses are applied to the J1 data to assess cyclicity and to evaluate the mechanisms that drive millennial- to multidecadal-scale variability during this portion of the last glaciation.

* Corresponding author. J.D. Mollard and Associates, Regina, SK, Canada, S4P 0R7. Fax: +1 306 352 8820.
E-mail address: cosford@jdmollard.com (J. Cosford).

0033-5894/$ – see front matter © 2010 University of Washington. Published by Elsevier Inc. All rights reserved.
doi:10.1016/j.yqres.2010.01.003

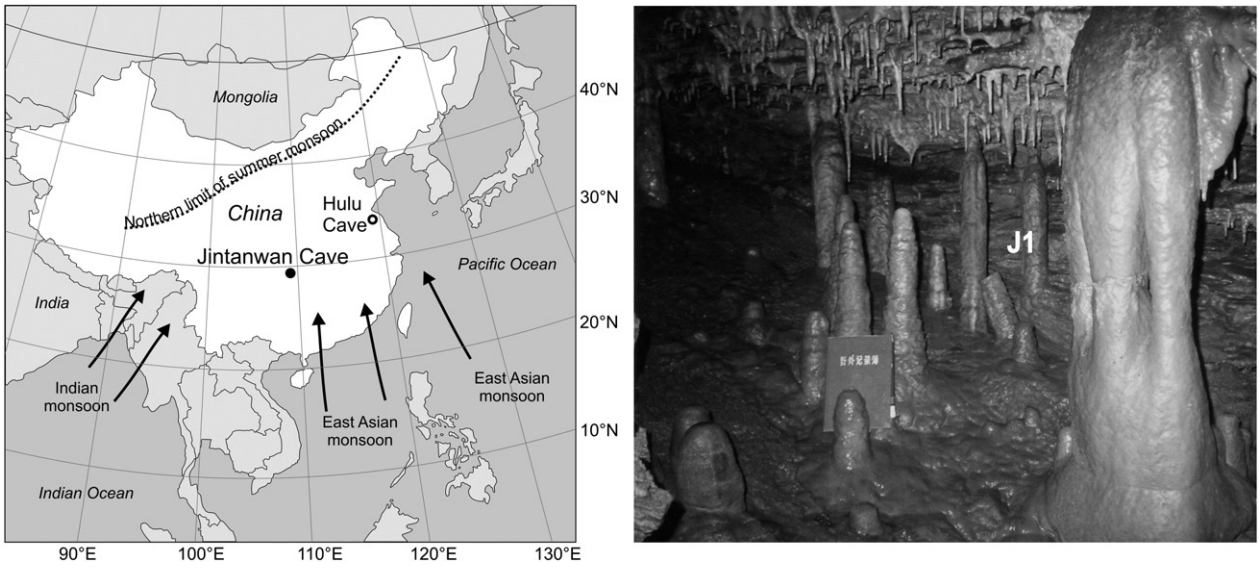

Figure 1. (A) Location of Jintanwan Cave, Hunan, China (left panel). Arrows show generalized modern East Asian and Indian monsoon winds. (B) Photograph of stalagmite J1 at the time of collection from Jintanwan Cave (right panel).

Location and modern climate

Jintanwan Cave (109°32′E, 29°29′N, elevation 460 m) is located near Bajin, Hunan Province, China (Fig. 1, left panel). Karstic terrain in this region developed in Paleozoic carbonates and features deeply incised plateaus with topographic relief of over 900 m. Entrance to the cave is 460 m above sea level. Stalagmite J1 was collected ~100 m from the entrance in the innermost chamber of the cave, which is decorated with a variety speleothems (Fig. 1, right panel). Climatic conditions in the region exhibit two distinct seasons associated with the Asian monsoon system and the annual migration of the intertropical convergence zone (ITCZ) in response to seasonal changes in insolation (Wang et al., 2005). During the summer monsoon season, from June to September, the ITCZ shifts northward and low atmospheric pressures over the continent draw warm and moist air masses from the tropical Pacific. From October to May, during the winter monsoon season, the ITCZ shifts southward and high atmospheric pressures over the continent drive cold and dry air masses southward from northern Siberia. Because of these seasonal changes in monsoonal circulation, summer rainfall provides the greatest contribution to total annual precipitation. Convergence of low- and mid-latitude air masses produces frontal weather systems that also influence the seasonality and amount of precipitation (Ge et al., 2007).

Materials and methods

Sample description

Stalagmite J1 is 42 cm high and has a maximum diameter of 5 cm (Fig. 2). The sample was halved and polished along the growth axis to check for visible indications of recrystallization, detrital accumulation, and depositional hiatuses. It consists primarily of brownish white to colourless calcite. Visible growth bands are observed throughout most of the section and vary in thickness on millimeter to sub-millimeter scales. Finer-scale microbanding was not observed using optical microscopy and UV luminescence. Detrital material was not observed in any of the bands. The primary structure of the calcite crystals and microbands appear well-preserved with no visible evidence for dissolution or recrystallization. Although most of the stalagmite appears to have grown continuously, there are a few irregular contacts and minor differences in colour that hint at brief cessations in growth. The age–depth relationship indicates a relatively uniform growth rate,

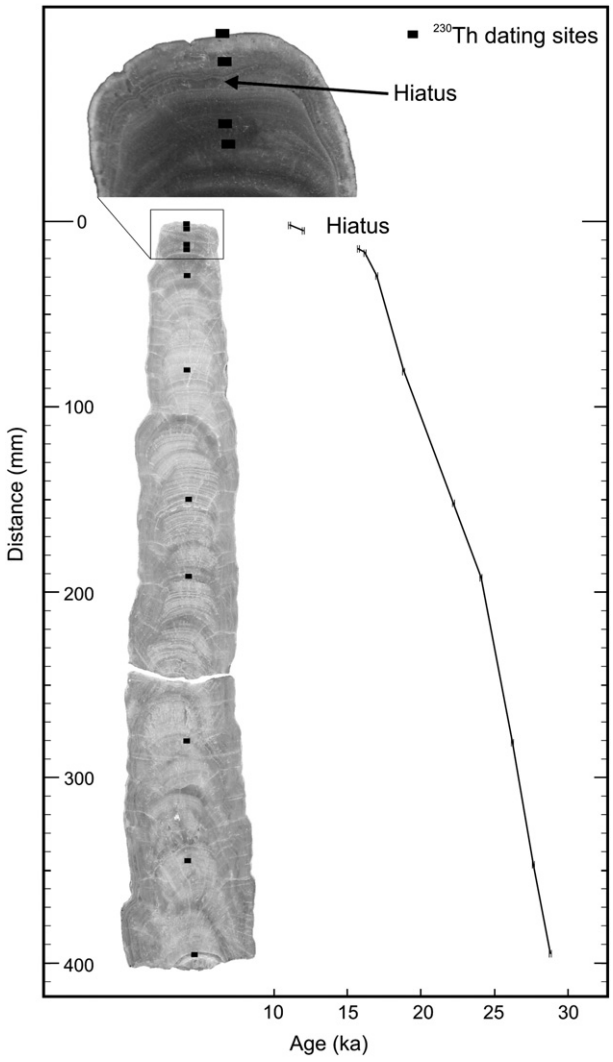

Figure 2. Photograph of stalagmite J1 with ^{230}Th age dates (ka) and growth rate.

https://doi.org/10.1016/j.yqres.2010.01.003 Published online by Cambridge University Press

with the exception of the uppermost portion from the top of the sample to a depth of 15 mm. The top age of the stalagmite is much younger than would be expected following a linear growth rate and indicates a likely depositional hiatus. Visual cues for a hiatus in this portion of the stalagmite include slight differences in colour and a change in the thickness and appearance of growth bands.

$^{230}Th/^{234}U$ dating

The $^{234}U/^{230}Th$ method of dating provided eleven ages from sites along the growth axis to establish chronological control of the isotopic records. Using a carbide burr, between 300 and 500 mg of powder was extracted for each sample from within individual stratigraphic horizons. Sample powder was prepared for isotopic analysis using the procedures for U and Th purification of Edwards et al. (1987). U and Th isotopes were then were then measured by inductively coupled plasma mass spectrometry (ICP-MS), as described by Shen et al. (2002), on a Finnigan-MAT element with a double focusing sector-field magnet and a single MasCom multiplier in the Isotope Laboratory of the Department of Geology and Geophysics, University of Minnesota. A continuous age model was constructed by linear interpolation of these dates. An initial $^{230}Th/^{232}Th$ atomic ratio of $(4.4 \pm 2.2) \times 10^{-6}$, representing Th isotopes in secular equilibrium with the bulk earth $^{232}Th/^{238}U$ value of 3.8 was used to correct for detrital Th contamination. Dates are reported with analytical errors at two standard deviations (2σ analytical error).

Analysis of $\delta^{18}O$

Sample extraction and isotopic measurements were performed at the Department of Geosciences, National Taiwan University. The stalagmite was cut into a thin slab and then the cut surface was polished with emery wheels and cleaned with deionized water. Using a standard dental drill, sample powder was manually extracted at 0.5-mm increments. Each powdered sample was dissolved in phosphoric acid (103% H_3PO_4) at 70°C to liberate CO_2, from which $\delta^{18}O$ and $\delta^{13}C$ measurements were made using a Kiel IV automated carbonate reaction device coupled with a Finnigan MAT 253 mass spectrometer. Delta values are reported with respect to the Vienna Pee Dee Belemnite (VPDB) standard. Isotope ratios were calibrated against the MAB working standard and were corrected for the effects of acid fractionation and ^{17}O contribution. Replicate samples demonstrated a precision of ± 0.06‰ for $\delta^{18}O$ and ± 0.03‰ for $\delta^{13}C$ (2σ).

Spectral and wavelet analyses

Several time-series techniques were performed to assess cyclical variations in the $\delta^{18}O$ data: (1) multi-taper method (MTM) utilizing the MTM-SSA Toolkit (http://www.atmos.ucla.edu/tcd/ssa/) (Ghil et al., 2002); (2) singular spectrum analysis (SSA) following modified routines in Matlab (Ghil et al., 2002 and Breitenberger unpubl.); (3) a modification of the Lomb-Scargle approach using the REDFIT package of Schulz and Mudelsee (2002); and (4) a continuous transform wavelet, using Morlet mother wavelets and procedures modified from Torrence and Campo (1998) and Grinsted et al. (2004), which permits simultaneously identification of variations in a signal in both the time and frequency domain. By applying multiple techniques and comparing the results, common periodicities can be more confidently identified and are unlikely to be artefacts of any one technique.

With the exception of the modified Lomb-Scargle approach, each technique requires input data to be evenly spaced in time. This was done by generating a denser set of points using a smoothing spline (Reinsch, 1967) and a very low degree of smoothing, as implemented in the TimeCurve software package (http://sil.usask.ca/software.htm), and then generating an evenly spaced data set using linear interpolation as implemented in a Matlab routine. Long-term trend (which has deleterious effects on frequency analysis) was removed from the data prior to MTM, SSA and wavelet spectral analysis using the first principal component in an initial pass through the SSA software. This approach is not applicable to the original, unevenly spaced data used with the REDFIT program. In this case, stationarity in the input data was achieved by first computing the 1st difference. Because the modified Lomb-Scargle approach uses the original, unevenly spaced data, it provides a check for artefacts introduced by interpolation of the data needed for the other techniques. Significant peaks were tested against a null hypothesis of a globally red noise background, estimated empirically from the first order auto-regressive [AR(1)] character of the data.

Results

The age model

The age model for stalagmite J1 is based on eleven ^{230}Th dates (Table 1) that are in chronological order and record a period of growth from ~11.0 to ~28.8 ka (Fig. 2). ^{238}U concentrations ranged from 1644 to 5293 ppb. $^{230}Th/^{232}Th$ atomic ratios ranged from 1199×10^{-6} to $11{,}515 \times 10^{-6}$, indicating that the sample contains very little detrital ^{230}Th. Nevertheless, corrections for initial ^{230}Th were made assuming an initial $^{230}Th/^{232}Th$ atomic ratio of $4.4 \pm 2.2 \times 10^{-6}$. With high uranium concentrations and minimal ^{230}Th contamination, the sample dates exhibited dating errors of typically better than 0.5%. Dating errors are reported to two standard deviations (2σ analytical error).

A continuous age model for the isotopic record was constructed by assigning each $\delta^{18}O$ and $\delta^{13}C$ value an age calculated by linear interpolation between the ^{230}Th dates. Errors for the interpolated ages were estimated by adding the linear weighted bounding age errors. While this approach provides a reasonable estimate of the interpolated age errors, the largest source of age uncertainty relates to the sub-sampling interval as this can span several decades. Throughout most of the record, from 28.8 to 16.2 ka the stalagmite appears to have grown continuously, with similar growth rates ranging from ~14 to 42 μm/yr and a median of 37 μm/yr. After 16.2 ka the stalagmite grew at a slower rate of ~5 μm/yr until a depositional hiatus at ~14.7 ka. The ^{230}Th dates at ~15.8 and ~12.0 ka span 1 cm and poorly constrain the timing of the hiatus located in between. For several $\delta^{18}O$ measurements made from this interval, ages were calculated using a linear extrapolation of the growth rates from the bounding ages to the apparent hiatus at 9.5 mm. This approach sets the timing of the depositional hiatus between ~14.7 and ~12.9 ka. After ~12.9 ka deposition resumed until ~11.0 ka when the stalagmite stopped growing.

$\delta^{18}O$ records

Sampling at a spatial resolution of 0.5 mm along the growth axis yielded a total of 783 $\delta^{18}O$ measurements that range in value from -4.5‰ to -7.9‰, with an average of -6.7‰. Figure 3 shows the $\delta^{18}O$ profile plotted against the linear age model. This approach of sampling at a constant spatial resolution resulted in uneven temporal resolution of approximately 12 yr between 28.8 and 24.1 ka, 24 yr between 24.1 and 18.8 ka, 14 yr between 18.8 and 17.7 ka, and 36 yr from 17.7 to 16.1 ka. After 16.1 ka, the temporal resolution drops to about 100 yr because of a slower growth rate, which then transitions into a period of depositional hiatus between ~14.7 and ~12.9 ka.

From the beginning of growth to ~25 ka $\delta^{18}O$ values remain relatively low with centennial-scale negative excursions at ~27.9 and ~29.5 ka that may represent Dansgaard-Oeschger events 3 and 4, respectively. From ~25 to 23 ka $\delta^{18}O$ values increase by about 1.5‰ but lack a clear expression of Heinrich event H2. After ~23 ka, $\delta^{18}O$ values exhibit a declining trend, with relatively low-amplitude fluctuations, leading to a period of low values between 19.2 and

https://doi.org/10.1016/j.yqres.2010.01.003 Published online by Cambridge University Press

Table 1
^{230}Th dating results for J1.

Sample number	Depth (mm)	^{238}U (ppb)	^{232}Th (ppt)	^{230}Th/^{232}Th (atomic x10^{-6})	δ^{234}U* (measured)	^{230}Th/^{238}U (activity)	^{230}Th age (yr) (uncorrected)	^{230}Th age (yr) (corrected)	$\delta^{234}U_{Initial}$** (corrected)	^{230}Th age (yr BP)*** (corrected)
J1-1	0.0	2821 ± 8.1	4938 ± 42	1321 ± 16	2034.8 ± 3.8	0.296 ± 0.0002	11136 ± 64	11093 ± 71	2116 ± 4.1	11037 ± 71
J1-2	5.0	5293 ± 15.0	23511 ± 244	1199 ± 13	2038.0 ± 3.8	0.323 ± 0.0013	12113 ± 55	12072 ± 62	2109 ± 4.0	12014 ± 62
J1-3	15.0	3263 ± 7.0	15376 ± 158	1476 ± 16	2071.3 ± 3.4	0.422 ± 0.0014	15854 ± 59	15811 ± 67	2166 ± 4.0	15754 ± 67
J1-4	17.0	1644 ± 0.1	2469 ± 25	4719 ± 48	2063.2 ± 0.6	0.43 ± 0.0002	16228 ± 10	16214 ± 12	2160 ± 0.6	16158 ± 12
J1-5	38.0	2904 ± 8	3105 ± 32	7055 ± 73	2000.0 ± 5	0.457 ± 0.0016	17722 ± 73	17712 ± 73	2103 ± 6	17656 ± 73
J1-6	81.0	2911 ± 8	2028 ± 21	11515 ± 122	2004.7 ± 6	0.486 ± 0.0016	18896 ± 79	18890 ± 79	2115 ± 6	18834 ± 79
J1-7	152.0	2388 ± 0.1	14353 ± 144	1575 ± 16	2037.7 ± 0.8	0.574 ± 0.0004	22318 ± 19	22262 ± 34	2170 ± 0.9	22206 ± 34
J1-8	192.0	2857 ± 9	7824 ± 79	3713 ± 38	2033.1 ± 6	0.616 ± 0.0024	24176 ± 116	24151 ± 117	2177 ± 7	24095 ± 117
J1-9	281.0	2159 ± 0.1	6391 ± 64	3638 ± 37	1974.6 ± 1	0.654 ± 0.0003	26307 ± 13	26280 ± 19	2127 ± 1	26224 ± 19
J1-10	346.0	2162 ± 0.1	5275 ± 53	4638 ± 47	1980.4 ± 1	0.687 ± 0.0003	27727 ± 14	27704 ± 18	2142 ± 1	27648 ± 18
J1-11	394.5	3196 ± 11.0	4425 ± 45	8286 ± 87	1914.0 ± 7	0.695 ± 0.0003	28875 ± 166	27704 ± 18	2077 ± 8	28805 ± 166

$\lambda_{230} = 9.1577 \times 10^{-6}$ Y^{-1}; $\lambda_{234} = 2.8263 \times 10^{-6}$ Y^{-1}; $\lambda_{238} = 1.55125 \times 10^{-6}$ Y^{-1}.
* $\delta^{234}U = ([^{234}U/^{238}U]_{active} - 1) \times 1000$.
** $\delta^{234}U_{Initial}$ calculated based on ^{230}Th age (T), i.e., $\delta^{234}U_{initial} = \delta^{234}U_{measured} \times e\lambda^{234 \times T}$. Corrected ^{230}Th ages assume an initial ^{230}Th/^{230}Th atomic ratio of $(4.4 \pm 2.2) \times 10^{-6}$. Those are the values for a material at secular equilibrium with the bulk earth ^{232}Th/^{238}U value of 3.8. Errors are 2σ.
*** BP stands for "Before Present" where the "Present" is defined as the year 1950 A.D.

17.4 ka (with a low of -7.1‰ at ~17.9 ka) that coincides with the timing of the LGM. This interval is followed by a progressive increase in δ^{18}O values that reach a high of -4.5‰ at ~15.8 ka, which corresponds within dating error to the timing of Heinrich event H1. Following the H1 event, δ^{18}O values decreased until reaching a hiatus at ~14.7 ka. Speleothem growth resumed after 12.6 ka, and the δ^{18}O record captures a large and abrupt decrease in values from -5.0‰ at ~11.7 ka to -7.0‰ at ~11.5 ka, which corresponds to the timing of the end of the Younger Dryas.

Time-series analysis

Spectral analyses using MTM, Lomb-Scargle, and SSA on the J1 δ^{18}O data yielded numerous significant frequencies above the 99%

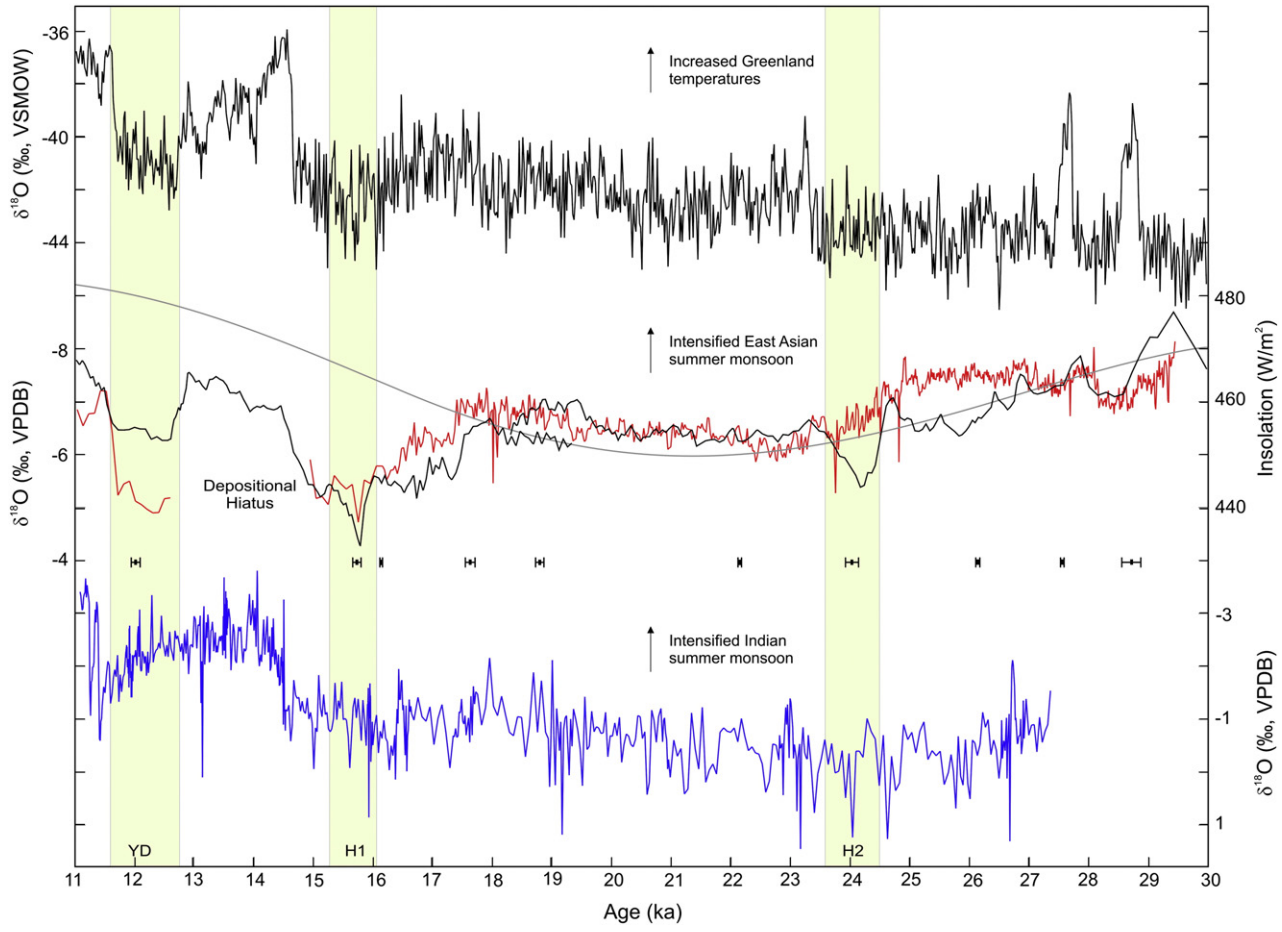

Figure 3. The δ^{18}O profile of stalagmite J1 with ^{230}Th ages and errors (2σ) (black bars) compared to the records of Hulu Cave (Wang et al., 2001) (thin black line beneath J1 line), Greenland ice core, NGRIP (Svensson et al., 2006) (black line), Moomi Cave (Shakun et al., 2007) (blue line), and averaged summer (June, July, August) insolation at 33°N (Berger, 1978) (grey line). Vertical green bars depict the Younger Dryas and Heinrich events (Bond et al., 1993).

https://doi.org/10.1016/j.yqres.2010.01.003 Published online by Cambridge University Press

confidence level relative to an AR(1)-based red noise spectrum and identify a broad band of significant cyclicity with period ranging from about 80–28 yr (Fig. 4). Most of these frequencies were common to at least two of the techniques, but only frequencies of ~54, ~44, ~39, and ~35 yr were common to all techniques. The Lomb-Scargle and SSA identified periodicities of, ~111, ~80, ~67and 60 yr that the MTM failed to identify. However, the MTM did identify a periodicity of 95 yr that may relate to either the ~111- or 80-yr periods. The only periods consistently identified by all techniques were ~54, ~44, ~39, and ~35 yr. Together these three frequencies along with others at 60, 52/50, 43/42, and 41/40 yr define a common range from ~40 to 60 yr. For cycles with shorter periods than ~35 yr, the MTM and SSA techniques yielded common periodicities of 30 and 24 yr that the Lomb-Scargle technique did not, suggesting that these frequencies may be an artefact of interpolation used to generate an evenly spaced time-series. These periods also approach the Nyquist frequency and are, therefore, not considered significant.

Wavelet analysis of the J1 record identifies a broad spectrum of high power, consistent with the other spectral analysis techniques, but the periodicity identified as significant extends to much longer times, making it difficult to specify individual periods (Fig. 5). Unlike many time series from climate data sets, stalagmite J1 shows remarkable continuity in 95% significance of the periodicity throughout the sample record. The wavelet graph also illustrates that some of the higher frequency cycles of less than about 35–40 yr identified by the other techniques are only identifiable in parts of the signal; elsewhere, the Nyquist frequency is too low to identify these periods.

Discussion

Interpretation of speleothem $\delta^{18}O$ values

Fluctuations in $\delta^{18}O$ values of speleothem J1 serve as a proxy for climatic changes in the hydrological cycle. Numerous fractionation effects in the hydrosphere are integrated in the $\delta^{18}O$ values of meteoric precipitation delivered to the cave system, including initial composition of the source water vapour, latent heat flux and water vapour transport, amount of rain out, temperature, and mixing of the air mass along the depositional pathway (Rozanski et al., 1993). Previous studies on the complex $\delta^{18}O$ systematics of precipitation in China show significant spatial and temporal variability in the dominant effect for a specific region (Johnson and Ingram, 2004). At mid- to high latitudes, beyond the northern limit of monsoonal circulation, precipitation $\delta^{18}O$ values correlate to surface air temperatures; whereas at low latitudes, within the influence of the Asian monsoon, precipitation $\delta^{18}O$ values reflect the amount of summer monsoon precipitation. Due to these observations of modern precipitation, speleothem $\delta^{18}O$ values in this region of China have largely been interpreted as a proxy for the intensity of summer monsoonal precipitation with lower $\delta^{18}O$ values during interstadial periods and higher $\delta^{18}O$ values during stadial periods (Wang et al., 2001; Yuan et al., 2004; Cheng et al., 2006; Wang et al., 2008). We observed the same correspondence between $\delta^{18}O$ values and stadial and interstadial periods in stalagmite J1.

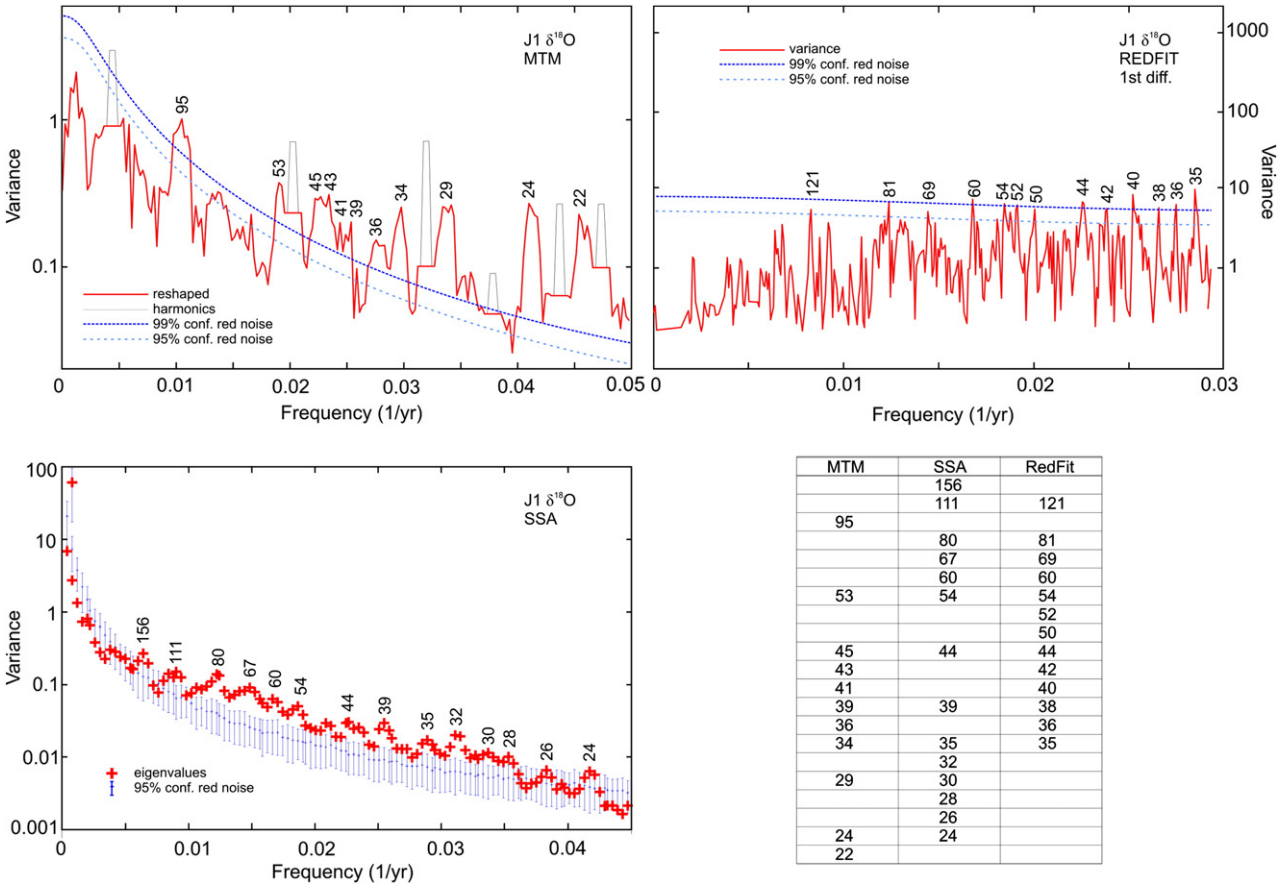

MTM	SSA	RedFit
	156	
	111	121
95		
	80	81
	67	69
	60	60
53	54	54
		52
		50
45	44	44
43		42
41		40
39	39	38
36		36
34	35	35
	32	
29	30	
	28	
	26	
24	24	
22		

Figure 4. Power spectra for the J1 $\delta^{18}O$ data set. (A) Multi-taper method (upper left). Time series was detrended by removing the principal component identified by SSA. Spectral peaks that are possible higher-degree harmonics of lower frequency oscillations were identified (thin lines) and omitted from the reshaped spectrum. 95% and 99% confidence limits relative to an AR(1) red noise spectrum. (B) REDFIT program (upper right). 95% and 99% confidence limits relative to an AR(1) red noise spectrum. (C) Singular spectrum analysis (lower left). 95% confidence limits (grey bars) for an AR(1) red noise spectrum were estimated by Monte Carlo simulations. Plus symbols above the 95% confidence bars are deemed significant. Major peaks are labelled with their periods.

https://doi.org/10.1016/j.yqres.2010.01.003 Published online by Cambridge University Press

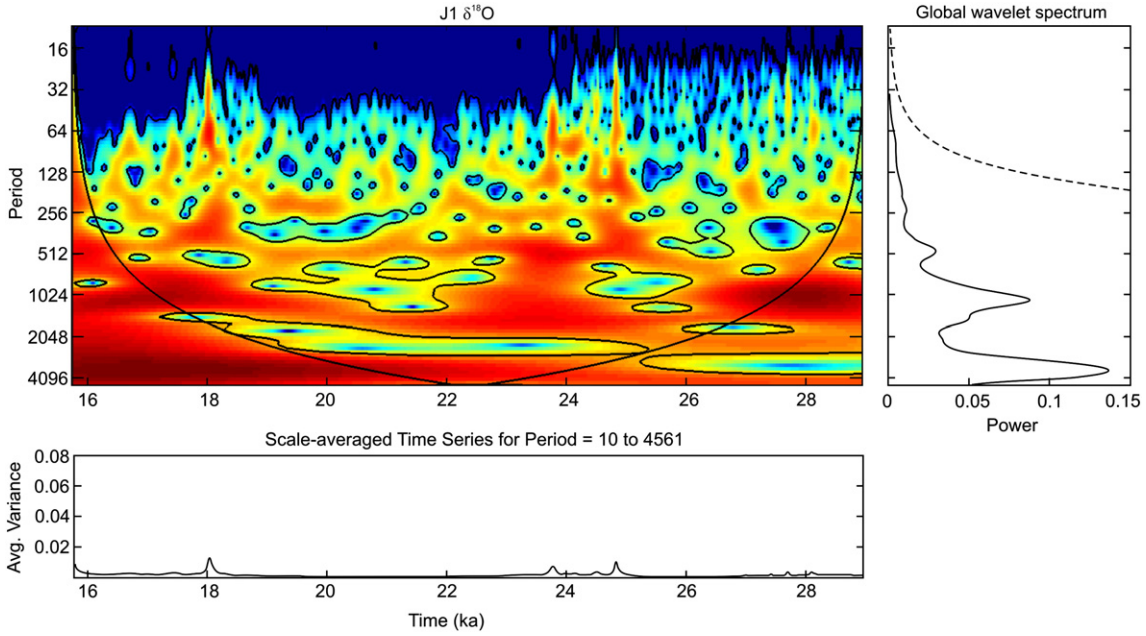

Figure 5. Continuous transform wavelet spectra for the detrended J1 $\delta^{18}O$ data. Spectral power (variance) is shown by colours ranging from deep blue (weak) to deep red (strong) and is plotted with period on the *y*-axis and age on the *x*-axis. Black cone delineates the upper boundary below which edge effects introduced by the computation method become important, thus limiting the degree of certainty with which identified frequencies may be interpreted. Irregular black curves delineate 95% confidence time-frequency regions in which the spectral strength is above that expected for an AR(1) red noise signal. Global wavelet spectrum (to right of coloured diagram) is a time-averaged summary of the wavelet spectra, and may be considered similar to spectra produced by other time-series analytical methods (MTM and REDFIT). Dashed curve is the global 95% confidence limit. The lower plot shows consistent average variance.

Recent studies have proposed more dynamic interpretations of speleothem $\delta^{18}O$ values to account for observed spatial variability (Hu et al., 2008). In particular, LeGrande and Schmidt (2009) used a water-isotope enabled, coupled atmosphere–ocean general circulation model to show that variability in atmospheric heat transport and water vapour flux dominates the meteoric $\delta^{18}O$ signal rather than changes in local precipitation amount. During periods of enhanced boreal seasonality and greater land–sea temperature contrasts, increased latent heat transport and a northward shift in the ITCZ lead to the delivery of more isotopically depleted water vapour exported from source regions in the tropical Indo-Pacific. Climate modelling also suggests that during stadial events, diminished Atlantic meridional overturning circulation and increased sea ice in the North Atlantic caused the ITCZ to shift southward and to produce meridional asymmetry in Hadley circulation, resulting in drier conditions in northern low latitudes (Chiang and Bitz, 2005).

Although most of the variability observed in the $\delta^{18}O$ record can be attributed to changes in the monsoon, at least part of the signal during this time period reflects dramatic changes in air temperature and global ice volume. Cave temperature affects fractionation between calcite and water (-0.23‰ per °C; O'Neil et al., 1969), but in eastern China this effect is typically overwhelmed by the large seasonal and interannual variations in $\delta^{18}O$ values of modern monsoonal precipitation. However, Wu et al. (2009) estimated that changes in air temperatures in eastern China during the interval from the LGM to the Holocene contributed a range of 1–1.9‰ to the $\delta^{18}O$ record of Hulu Cave.

Due to the preferential removal of ^{16}O from the oceans and then storage on land in glacial ice, seawater $\delta^{18}O$ values during the LGM were approximately 1.0‰ higher than today (Schrag et al., 1996). As global ice volumes shrank from the LGM, relatively depleted water returned to the ocean and $\delta^{18}O$ values decreased. Because air masses derive moisture from the oceans, this decrease in ocean $\delta^{18}O$ values should be reflected in the meteoric precipitation that contributed to the J1 $\delta^{18}O$ record. To quantify the decrease in ocean $\delta^{18}O$ values as the ice sheets retreated, Dykoski et al., (2005) assumed a linear relationship between sea level and ocean $\delta^{18}O$ values and determined that ocean $\delta^{18}O$ had decreased ~0.15‰ by 16 ka. Based on these changes in ocean $\delta^{18}O$ values, the ice volume effect may account for ~10% of the range of values expressed in the J1 $\delta^{18}O$ record over this period.

Local cave effects on the $\delta^{18}O$ record

Although interpreted as a proxy for changes in the hydrological cycle, local cave effects can blur the primary climatic signal expressed in speleothem $\delta^{18}O$ values (Fairchild et al., 2006). Since the seminal work of Hendy (1971) much attention has been paid to whether calcite precipitates in isotopic equilibrium with drip waters. Seldom can equilibrium and kinetic effects be constrained and for relatively long-term studies, such as this, it is difficult to justify the assumptions of equilibrium (Mickler et al., 2004; Mickler et al., 2006). Nevertheless, where the cave system remains unchanged over time (rates of erosion and uplift, cave roof thickness, etc.) local effects that might alter the climatic signal are assumed constant. Over the timescales and temporal resolutions reported in this study, the Jintanwan Cave system retained the relative local cave effects on the climatic signal. Replicate $\delta^{18}O$ records of two stalagmites from the same cave would indicate preservation of a primary climatic signal that remained relatively unaltered by secondary effects unique to each stalagmite (Dorale et al., 1998). Without a second stalagmite from Jintanwan Cave, however, the J1 record was compared to Hulu Cave (Wang et al., 2001; Wu et al., 2009). These records show an overall correspondence that suggests the speleothem $\delta^{18}O$ values faithfully recorded changes in meteoric precipitation during this interval and were not significantly altered by local cave processes.

The East Asian monsoon and global climatic linkages

The $\delta^{18}O$ record of stalagmite J1 exhibits correspondence to Northern Hemisphere insolation and captures significant multi-millennial to multi-decadal variability that resembles the timing

https://doi.org/10.1016/j.yqres.2010.01.003 Published online by Cambridge University Press

and pattern of changes in other Asian stalagmite records and the Greenland ice cores. Comparisons of the J1 record to Hulu Cave (Wang et al., 2001; Wu et al., 2009), Moomi Cave (Shakun et al., 2007), and the NGRIP (Svensson et al., 2006) ice core are shown in Figure 3. Although the $\delta^{18}O$ values and seasonal patterns of modern precipitation in Hunan differ from those at Nanjing, the J1 speleothem record exhibits absolute $\delta^{18}O$ values and overall trends quite similar to those from Hulu Cave. This observation implies synchronicity in the major paleoclimatic events within regions influenced by the East Asian monsoon. Nevertheless, there are differences between these records, most notably J1 exhibits a much more positive excursion during the Younger Dryas event, with similar values to those during H1, and does not capture a prominent expression of the H2 event.

The Chinese stalagmite records of the East Asian monsoon correlate closely with the Greenland ice cores and indicate a tight coupling to climatic conditions in the North Atlantic. Intensified East Asian summer monsoonal circulation correlates with warmer temperatures over Greenland, whereas a weaker summer monsoon and strengthened winter monsoon correlate to periods of colder temperatures over Greenland. Numerous multidecadal-scale fluctuations observed in the records appear correlative, but different regional responses, local cave conditions, and imprecision in the age models limit correlations on these shorter time scales.

Comparisons between the J1 record of the East Asian monsoon and stalagmite M1–5 from Moomi Cave, Socotra Island, in the northwest Indian Ocean (Shakun et al., 2007) provide an opportunity to evaluate the linkages between the East Asian and Indian monsoon systems. That the two subsystems would exhibit similar fluctuations in strength and character is expected as both respond to seasonal changes in atmospheric pressure gradients between the Asian landmass and surrounding oceans. Nevertheless, differences between the two monsoon subsystems exist in the relative strengths of the winter and summer monsoonal circulation and in the sensitivity to internal feedback mechanisms due to contrasting geographic boundary conditions (Wang et al., 2003). Differences in the location of these two sites also influence the delivery of precipitation associated with seasonal migration of the ITCZ. Specifically, the ITCZ shifts northward over eastern Asia only during the boreal summer, but at Socotra Island annual migration of the ITCZ over the island in early summer and again in late fall produces a bimodal distribution of rainfall.

Overall, there are similar general trends on multi-millennial time scales expressed in the J1 and Moomi Cave records. Both stalagmites demonstrate weakening summer monsoonal circulation prior to Heinrich event H2 and into the LGM, followed by a strengthening to ~19 ka. After this time, the two records diverged, as the East Asian monsoon weakened to a low coincident with the cooling associated with H1, while the Indian monsoon continued to strengthen and remained relatively strong. Expression of H1 in the J1 and Hulu Cave records is much more pronounced than in the Moomi Cave record or even the Greenland ice cores. The Indian monsoon may not have responded strongly to Heinrich event H1 because increasing solar insolation at this time may have allowed monsoonal circulation to remain strong (Shakun et al., 2007). Climate modelling results also suggest that a reduction in Atlantic meridional overturning circulation and expansion of sea ice in the North Atlantic caused the ITCZ to shift southward and to remain longer over Socotra Island (Chiang and Bitz, 2005).

East Asian monsoon during the LGM

The LGM occurred between 23 and 19 ka, when high-latitude ice sheets reached their greatest volume (Yokoyama et al., 2000) and Northern Hemisphere isolation was at a minimum (Berger, 1978). The J1 record indicates that the East Asian summer monsoon weakened in the early stage and then strengthened in the latter stage of the LGM, which is consistent with the records of other Chinese stalagmites (Wu et al., 2009). The East Asian summer monsoon was relatively weak between 23 and 20 ka as summer insolation at northern latitudes reached a minimum. Accumulating ice sheets in the Northern Hemisphere initiated an albedo-temperature feedback mechanism that weakened the summer monsoon, while higher pressures over the ice sheets intensified anticyclonic circulation and bolstered westerly flow of cold and dry winds that increased the Siberian High and strengthened the winter monsoon (Ding et al., 1995). As a result, the Siberian High persisted longer into the spring and summer, perhaps becoming perennial, and thus diminished the strength of the summer monsoon. Under these conditions, diminished summer monsoonal precipitation and a greater ice volume effect on the oceanic moisture source contributed to the higher $\delta^{18}O$ values.

Beginning around ~20.0 ka, the summer monsoon strengthened gradually before peaking between 19.2 and 17.4 ka, as indicated by the relatively low $\delta^{18}O$ values recorded in stalagmite J1. This reversal in the intensity of the summer monsoon follows a precessional-driven rise in northern summer insolation and corresponds to warmer temperatures at both high and low latitudes (Koutavas et al., 2002) and to a decrease in global ice volume accompanied by a rise in sea level (Yokoyama et al., 2000). Strengthened summer monsoonal circulation at this time may reflect reorganizations of the North Atlantic thermohaline circulation (Clark et al., 2002) and changes in tropical ocean–atmosphere dynamics (Clement et al., 1999). Koutavas et al. (2002) reported that sea-surface temperatures in the tropical Pacific exhibited an El Nino-like pattern during the LGM followed by a La Nina-like pattern during deglaciation. Wu et al. (2009) proposed that the East Asian summer monsoon at this time strengthened in response to increased meridional circulation associated with a La Nina-like pattern in a super-ENSO system. The $\delta^{18}O$ values for this time are similar to those at the transition into the Holocene, but the relatively cooler and drier conditions should have resulted in weaker monsoon intensity. This observation suggests that the low $\delta^{18}O$ values reflect the contribution of other processes. In particular, sea levels lowered by ~120 m relative to present during the LGM, shifting the coastline of eastern China hundreds of kilometers eastward and exposing extensive areas of the continental shelf (Winkler and Wang, 1993). Mainland climatic conditions became more continental (drier and cooler) and much of the precipitation associated with the summer monsoon would have fallen on the then exposed continental shelf, causing an apparent reduction in precipitation at the cave site and contributing to lower $\delta^{18}O$ values at sites farther inland.

Synchronous climate change during Heinrich event H1

Previous studies of Chinese stalagmites have demonstrated that first-order trends in $\delta^{18}O$ values follow summer insolation curves (averaged over June, July, and August) at northern mid- to high latitudes (Wang et al., 2008). However, the behaviour of the East Asian monsoon after the LGM marks a significant departure from this relationship between orbital forcing of summer insolation and long-term trends in the strength of summer monsoonal circulation (Wang et al., 2001). Following the LGM, the relatively strengthened East Asian summer monsoon weakened and climatic conditions deteriorated, even as Northern Hemisphere summer insolation increased. In the J1 record, the weakest circulation of the East Asian summer monsoon since the LGM occurred at ~15.8 ka, when the North Atlantic and northern high latitude regions suffered cold and dry conditions associated with Heinrich event H1. The expression of this event in the J1 record matches remarkably well to that of the Hulu Cave record (Wang et al., 2001), and Zhou et al. (2008) note that the timing and pattern of this event in several Chinese stalagmite records indicate synchronous climatic changes across monsoonal China.

That the East Asian summer monsoon weakened at this time suggests a more sensitive response to air temperatures and oceanic

https://doi.org/10.1016/j.yqres.2010.01.003 Published online by Cambridge University Press

circulation in the North Atlantic than to insolation forcing at high northern latitudes. The hemispheric synchronicity demonstrated between the North Atlantic and East Asia during H1 implies a rapid atmospheric transfer of the climatic signal. During the H1 event, icebergs discharged into the North Atlantic disrupted the meridional overturning circulation, causing air temperatures to plummet throughout the region. These cold air temperatures propagated rapidly to East Asia via westerly winds and enhanced the winter land–sea pressure gradient that drives winter monsoonal circulation (Porter and An, 1995).

Deglaciation and the transition to the Holocene

Stalagmite J1 displays an incomplete deglacial record of the East Asian monsoon, owing to a depositional hiatus between ~14.7 and ~12.9 ka. Although lacking an expression of the Bølling/Allerød and the transition into the Younger Dryas, the rapid drop in $\delta^{18}O$ values at ~11.5 ka captures the end of the Younger Dryas and the beginning of the Holocene. The timing of this transition agrees within error to that of Hulu Cave (Wang et al., 2001) and the Greenland ice cores (Rasmussen et al., 2006). The Younger Dryas appears to have originated in the North Atlantic, as deglaciation released freshwater that triggered collapse of Atlantic thermohaline circulation and caused temperatures to plummet over Greenland (McManus et al., 2004). The resulting large-scale changes in oceanic and atmospheric circulation propagated the climatic signal to East Asia and weakened summer monsoonal circulation. The synchronicity and abruptness of this event supports a role for atmospheric teleconnections between Greenland temperatures and the East Asian monsoon. The $\delta^{18}O$ values in the J1 record near the end of this interval are almost as high as during Heinrich event H1, when Greenland climatic conditions were extremely cold and dry and the East Asian monsoon was severely weakened. This differs from other Asian stalagmite records that show relatively less weakening of the Asian monsoon during the Younger Dryas because the summer insolation values diminished the effects of glacial boundary forcing. Nevertheless, these observations demonstrate that even more so than insolation forcing, changes in Northern Hemisphere ice volume and temperature during deglaciation strongly regulated the intensity of the East Asian monsoon.

The low $\delta^{18}O$ values in the J1 record since ~11.5 ka reflect insolation forcing of enhanced East Asian summer monsoonal circulation in the early Holocene. At the end of the Younger Dryas, high summer insolation values and changed glacial boundary conditions drove an abrupt strengthening of the East Asian summer monsoon that marked the transition into the Holocene. Since then, insolation forcing has been the primary driver of long-term trends in the East Asian summer monsoon.

Periodicity in the East Asian monsoon

Periodic fluctuations expressed in the J1 $\delta^{18}O$ values may suggest a response of the Asian monsoon to cyclical variations in solar activity and to changes in atmospheric and oceanic circulation. The J1 record contains periodic fluctuations of 80–95 yr that may reflect the well-known Gleissberg cycle in solar activity of 88 yr. Other multidecadal cycles identified in the J1 record may correspond to periods identified in the INTCAL04 data at 110, 67, and 50 yr (Reimer et al., 2004). These results are consistent with evidence presented by Prasad et al. (2004) for solar forcing of decadal-scale climate variability during MIS 2. Several periodicities identified in the J1 $\delta^{18}O$ data fall in the range of 40–60 yr, which have also been linked to changes in solar activity and to the Pacific Decadal Oscillation (Minobe, 1997) and the North Atlantic Oscillation (Gimeno et al., 2003). Cyclical fluctuations with similar periods are also well-expressed in Holocene stalagmite records from China (Cosford et al., 2008).

Conclusions

The patterns and trends expressed in the $\delta^{18}O$ record of stalagmite J1 offer insights on the behaviour of the East Asian monsoon during the late glacial and deglaciation. Comparisons to other Asian stalagmite records and to the Greenland ice cores suggest that the timing and magnitude of changes in the East Asian monsoon were broadly synchronous, and that these changes are linked by atmospheric and oceanic mechanisms to climatic conditions around the North Atlantic. During the LGM, the East Asian summer monsoon first weakened and then strengthened in response to changes in insolation and ice volume. Although insolation continued to increase after the LGM, the East Asian summer monsoon weakened until reaching a minimum during Heinrich event H1 in response to changes in air temperature and oceanic circulation around the North Atlantic. The synchronicity of climatic changes associated with this event supports an atmospheric mechanism to rapidly transfer the climatic signal. Stalagmite J1 ceased to grow between ~14.7 and ~12.9 ka so most of the deglacial monsoon record is missing, but a rapid drop in $\delta^{18}O$ values at 11.5 ka marks an abrupt end of the Younger Dryas and the transition into the Holocene. Centennial- and decadal-scale fluctuations in the J1 data, evaluated by spectral and wavelet analyses, exhibited periodicities that correspond to solar frequencies and to oscillations in atmospheric and oceanic circulation, but are intermittent throughout the record.

Acknowledgments

NSERC Discovery grants to H.Q. funded this research. We thank three anonymous reviewers for providing thoughtful comments that improved the original manuscript.

References

Berger, A., 1978. Long-term variations of daily insolation and quaternary climate changes. Journal of the Atmospheric Sciences 35, 2362–2367.
Bond, G., Broecker, W., Johnsen, S., McManus, J., Labeyrie, L., Jouzel, J., Bonani, G., 1993. Correlations between climate records from North Atlantic sediment and Greenland ice. Nature 365, 143–147.
Cheng, H., Edwards, L., Wang, Y., Kong, X., Ming, Y., Kelly, M., Wang, X., Gallup, C., Liu, W., 2006. A penultimate glacial monsoon record from Hulu Cave and two phase glacial terminations. Geology 34, 217–220.
Chiang, J., Bitz, C., 2005. Influence of high latitude ice cover on the marine Intertropical Convergence Zone. Climate Dynamics 25, 477–496.
Clark, P., Pisias, N., Stocker, T., Weaver, A., 2002. The role of thermohaline circulation in abrupt climate change. Nature 415, 863–869.
Clement, A., Seager, R., Cane, M., 1999. Orbital controls on the El Nino/Southern oscillation and the tropical climate. Paleoceanogrpahy 14 (4), 441–456.
Cosford, J., Qing, H., Eglington, B., Mattey, D., Yuan, D., Zhang, M., Cheng, H., 2008. East Asian monsoon variability since the Mid-Holocene recorded in a high-resolution, absolute-dated aragonite speleothem from eastern China. Earth and Planetary Science Letters 275, 296–307.
Ding, Z., Liu, T., Rutter, N., Yu, Z., Guo, Z., Zhu, R., 1995. Ice-volume forcing of East Asian winter monsoon variations in the past 800,000 years. Quaternary Research 44, 149–159.
Dorale, J., Edwards, R., Ito, E., Gonzalez, L., 1998. Climate and vegetation history of the midcontinent from 75–25 ka: a speleothem record from Crevice Cave, Missouri, USA. Science 282, 1871–1874.
Dykoski, C., Edwards, R., Cheng, H., Yuan, D., Cai, Y., Zhang, M., Lin, Y., Qing, J., An, Z., Revenaugh, J., 2005. A high-resolution, absolute-dated Holocene and deglacial Asian monsoon record from Dongge Cave. China. Earth and Planetary Science Letters 233, 71–86.
Edwards, R., Chen, J., Wasserburg, G., 1987. ^{238}U–^{234}U–^{230}Th–^{232}Th systematics and the precise measurement of time over the past 500,000 years. Earth and Planetary Science Letters 81, 175–192.
Fairchild, I., Smith, C., Baker, A., Fuller, L., Spotl, C., Mattey, D., McDermott, F., E.I.M.F., 2006. Modification and preservation of environmental signals in speleothems. Earth-Science Reviews 75, 105–153.
Ge, Q., Guo, F., Zheng, J., Hao, Z., 2007. Meiyu in the middle and lower reaches of the Yangtze River since 1736. Chinese Science Bulletin 52, 1–8.
Ghil, M., Allen, R., Dettinger, M., Ide, K., Kondrashov, D., Mann, M., Robertson, A., Saunders, A., Tian, Y., Varadi, F., Yiou, P., 2002. Advanced spectral methods for climatic time series. Reviews of Geophysics 40 (1), 3.1–3.41. doi:10.1029/2000RG000092.
Gimeno, L., de la Torre, L., Nieto, R., Garcia, R., Hernandez, E., Ribera, P., 2003. Changes in the relationship NAO-Northern Hemisphere temperature due to solar activity. Earth and Planetary Science Letters 206, 15–20.

https://doi.org/10.1016/j.yqres.2010.01.003 Published online by Cambridge University Press

Grinsted, A., Moore, J., Jevrejeva, S., 2004. Application of the cross wavelet transform and wavelet coherence to geophysical time series. Nonlinear Processes Geophys 11, 561–566.
Hendy, C., 1971. The isotopic geochemistry of speleothems: I. The calculation of the effects of different modes of formation on the isotopic composition of speleothems and their applicability as palaeoclimatic indicators. Geochimica et Cosmochimica Acta 35, 801–824.
Hu, C., Henderson, G., Huang, J., Xie, S., Sun, Y., Johnson, K., 2008. Quantification of Holocene Asian monsoon rainfall from spatially separated cave records. Earth and Planetary Science Letters 266, 221–232.
Johnson, K., Ingram, B., 2004. Spatial and temporal variability in the stable isotope systematics of modern precipitation in China: implications for paleoclimate reconstructions. Earth and Planetary Science Letters 220, 365–377.
Koutavas, A., Lynch-Stieglita, J., Marchitto, T., Sachs, J., 2002. El Nino-like pattern in ice age tropical Pacific sea-surface temperature. Science 297, 226–230.
McManus, J., Francois, R., Gherardi, J., Keigwin, L., Brown-Leger, S., 2004. Collapse and rapid resumption of Atlantic meridional circulation linked to deglacial climate changes. Nature 428, 834–837.
Mickler, P., Banner, J., Stern, L., Asmerom, Y., Edwards, R., Ito, E., 2004. Stable isotope variations in modern tropical speleothems: evaluating equilibrium vs. kinetic effects. Geochimica et Cosmochimica Acta 68, 4381–4393.
Mickler, P., Stern, L., Banner, J., 2006. Large kinetic isotope effects in modern speleothems. Geological Society of America Bulletin 188 (1-2), 65–81.
Minobe, S., 1997. A 50-70 year climatic oscillation over the North Pacific and North America. Geophysical Research Letters 24, 683–686.
O'Neil, J., Clayton, R., Mayeda, T., 1969. Oxygen isotope fractionation in divalent metal carbonates. Journal of Chemical Physics 30, 5547–5558.
Porter, S., An, Z., 1995. Correlation between climate events in the North Atlantic and China during the last glaciation. Nature 375, 305–308.
Prasad, S., Vos, H., Negendank, J., Waldmann, N., Goldstein, S., Stein, M., 2004. Evidence from Lake Lisan of solar influence on decadal- to centennial-scale climate variability during marine oxygen isotope stage 2. Geology 32 (7), 581–584.
Rasmussen, S., Andersen, K., Svensson, A., Steffensen, J., Vinther, B., Clausen, H., Siggaard-Andersen, M., Johnsen, S., Larsen, L., Dahl-Jensen, D., Bigler, M., Röthlisberger, R., Fischer, H., Goto-Azuma, K., Hansson, M., Ruth, U., 2006. A new Greenland ice core chronology for the last glacial termination. Journal of Geophysical Research 111, D06102. doi:10.1029/2005JD006079.
Reimer, P., Baillie, M., Bard, E., Bayliss, A., Beck, J., Bertrand, C., Blackwell, P., Buck, C., Burr, G., Cutler, K., Damon, P., Edwards, R., Fairbanks, R., Friedrich, M., Guilderson, T., Hogg, A., Hughen, K., Kromer, B., McCormac, G., Manning, S., Ramsey, C., Reimer, R., Remmele, S., Southon, J., Stuiver, M., Talamo, S., Taylor, F., Van der Plicht, J., Weyhenmeyer, C., 2004. INTCAL04 terrestrial radiocarbon age calibration, 0-26 cal kyr BP. Radiocarbon 46, 1029–1058.
Reinsch, C., 1967. Smoothing by spline functions. Numerische Mathematik 10, 177–183.
Rozanski, K., Araguas-Araguas, L., Gonfiantini, R., 1993. Isotopic patterns in modern global precipitation. In: Swart, P.K., et al. (Ed.), Climate Change in Continental Isotopic Records. American Geophysical Union Monograph 78, Washington, pp. 1–36.
Schrag, D., Hampt, G., Murray, D., 1996. Pore fluid constraints on the temperature and oxygen isotopic composition of the glacial ocean. Science 272, 1930–1932.
Schulz, M., Mudelsee, M., 2002. REDFIT: estimating red-noise spectra directly from unevenly spaced paleoclimatic time series. Computers & Geosciences 28, 421–426.
Shakun, J., Burns, S., Fleitmann, D., Kramers, J., Matter, A., Al-Subary, A., 2007. A high-resolution, absolute-dated deglacial speleothem record of Indian Ocean climate from Socotra Island, Yemen. Earth and Planetary Science Letters 259, 442–456.
Shen, C., Edwards, R., Cheng, H., Dorale, J., Thomas, R., Moran, S., Weinstein, S., Edmonds, H., 2002. Uranium and thorium isotopic concentration measurements by magnetic sector inductively coupled plasma mass spectrometry. Chemical Geology 185, 165–178.
Svensson, A., Andersen, K., Bigler, M., Clausen, H., Dahl-Jensen, D., Davies, S., Johnsen, S., Muscheler, R., Rasmussen, S., Rothlisberger, R., Steffensen, J, Vinther, B., 2006. The Greenland Ice Core Chronology 2005, 15-42 ka. Part 2: Comparison to other records. Quaternary Science Reviews 25, 3258–3267.
Torrence, C., Compo, G., 1998. A practical guide to wavelet analysis. Bulletin of the American Meteorological Society 79, 61–78.
Wang, B., Clemens, S., Liu, P., 2003. Contrasting the Indian and East Asian monsoons: implications on geologic timescales. Marine Geology 201, 5–21.
Wang, P., Clemens, S., Beaufort, L., Braconnot, P., Ganssen, G., Jian, Z., Kershaw, P., Sarnthein, M., 2005. Evolution and variability of the Asian monsoon system: state of the art and outstanding issues. Quaternary Science Reviews 24 (5-6), 595–629.
Wang, Y., Cheng, H., Edwards, R., An, Z., Wu, J., Shen, C., Dorale, J., 2001. High-resolution absolute-dated late Pleistocene monsoon record from Hulu Cave, China. Science 294, 2345–2348.
Wang, Y., Cheng, H., Edwards, R., He, Y., Kong, X., Shao, X., Chen, S., Wu, J., Jiang, X., Wang, X., An, Z., 2008. Millennial- and orbital-scale changes in the East Asian monsoon over the past 224,000 years. Nature 451, 1090–1093.
Winkler, M., Wang, P., 1993. The Late-Quaternary vegetation and climate of China. In: Wright, H., Kutzbach, J., Webb, T., Ruddiman, W., Street-Perrott, F., Bartlein, P. (Eds.), Global climates since the Last Glacial Maximum. University of Minnesota Press, p. 569.
Wu, J., Wang, Y., Cheng, H., Edwards, L., 2009. An exceptionally strengthened East Asian summer monsoon event between 19.9 and 17.1 ka BP recorded in a Hulu stalagmite. Science in China Series D: Earth Sciences 52 (3), 360–368.
Yokoyama, Y., Lambeck, K., DeDecker, P., Johnston, P., Fifield, L., 2000. Timing of the Last Glacial Maximum from observed sea-level minima. Nature 406, 713–716.
Yuan, D., Cheng, H., Edwards, R., Dykoski, C., Kelly, M., Zhang, M., Qing, J., Lin, Y., Wang, Y., Wu, J., Dorale, J., An, Z., Cai, Y., 2004. Timing, duration, and transitions of the Last Interglacial Asian monsoon. Science 304, 575–578.
Zhou, H., Zhao, J., Feng, Y., Gagan, M., Zhou, G., Yan, J., 2008. Distinct climate change synchronous with Heinrich event one, recorded by stable oxygen and carbon isotopic compositions in stalagmites from China. Quaternary Research 69, 306–315.